JOURNAL OF PROPULSION AND POWER
Vol. 13, No. 5, September–October 1997

Analytical Solution of the Type IV Shock Interaction

Michael J. Frame* and Mark J. Lewis†
University of Maryland, College Park, Maryland 20742

An analytical model for the type IV shock interaction in high Mach number, calorically perfect air is developed. The model solves the flowfield around the transmitted shock, using the oblique shock relations, and the flow inside the jet, using Prandtl–Meyer waves. The length of the transmitted shock and jet geometry are derived explicitly by calculating the shape of the bow shocks using a continuity methodology. Unlike previous analytical methods, no empirical or experimental data on the interaction are required. The model for the jet impingement gives a prediction for the location and value of the peak pressure on the cylinder. Comparison with experimental results shows good agreement for the impingement location, peak pressure, and shock shapes, and the calculation is performed very quickly with minimal computing resources. A parametric study is conducted, demonstrating the variation of key interaction results such as peak pressure, impingement location and lengths of the transmitted shock, and the terminating shock of the jet, as a result of impinging shock location and strength, freestream Mach number, or cylinder radius. Many trends between the dependent and independent variables in this study were apparent, providing useful and insightful results for design purposes.

Nomenclature

A = area, per unit depth
C_p = pressure coefficient
k = shock equation constant
L = distance in shock detachment theory or length
M = Mach number
P = pressure
r = cylinder radius
x, y = spatial coordinates
x_0 = coordinate in shock detachment theory
β = constant, $\sqrt{M^2 - 1}$
γ = ratio of specific heats
$\Delta\theta$ = flow deflection between jet sections
δ = shock standoff distance
η = angle of shock-layer sonic line
θ, λ = angular measurement or flow angle
μ = Mach angle
ν = Prandtl–Meyer function
Π = total pressure ratio
σ = isentropic contraction ratio
Φ = constant, Eq. (20)
ϕ, ς = wave angle

Subscripts

A, B, C = points A, B, C
d = maximum wedge angle
i = impinging shock
imp = jet impingement
S = sonic point behind shock or sonic line
S_2 = sonic line between T and SB
SB = sonic point on body
stag = stagnation region
T = terminating shock or point T
$T1, T2$ = portions of terminating shock
t = transmitted shock
w = Prandtl–Meyer wave
0 = total conditions
1 = region below impinging shock
2, 3 = regions adjacent to jet
4, 5, 6 = regions inside supersonic jet
∞ = freestream conditions
$\hat{}$ = variables in the $(\hat{x}, \hat{y})$ plane

Presented as Paper 96-2548 at the AIAA/ASME/SAE/ASEE 32nd Joint Propulsion Conference, Lake Buena Vista, FL, July 1–3, 1996; received Oct. 5, 1996; revision received March 31, 1997; accepted for publication April 10, 1997.

*Graduate Research Assistant, Department of Aerospace Engineering. Student Member AIAA.

†Associate Professor, Department of Aerospace Engineering. Associate Fellow AIAA.

Introduction

THE problem of shock waves from different families intersecting in a supersonic or hypersonic flow is one of great interest, both in fluid dynamics and vehicle design. For example, on a hypersonic vehicle, there could be such intersections between the nose shock and engine cowl, wing, or fin leading-edge bow shocks. Other examples include shock waves emanating from attached stores, pylons, fuel injectors, control surfaces, and indented body contours. From a practical point of view, it is desirable for vehicle designers to be able to predict these interactions and their effects. From an intellectual point of view, it is desirable to understand the interactions as fluid phenomena and how they differ from the noninteracting cases.

Many of the previous examples involve a straight, oblique shock wave intersecting a curved, detached shock. Edney[1] characterized six such interactions (types I–VI), depending on where the intersection occurs on the curved bow shock. Some refinements to these classifications have been made subsequently, but the basic six still demonstrate the range of phenomena observed, including shock-wave–boundary-layer interactions, expansion fan–boundary-layer interactions, shear-layer impingement, and supersonic jet grazing and impingement.

A desirable feature of airframe–engine-integrated hypersonic vehicles is to have the oblique shock generated by the vehicle nose intersect the cowl lip of the engine intake. This type of intersection would typically result in a type III or IV interaction. A type IV interaction (Fig. 1) occurs when the oblique shock intersects with the region around the most normal part of the bow shock. In this paper, the impinging shock is drawn approaching from the lower, left quadrant of the flowfield, with the flow approaching from the left. The cowl lip is represented by a cylinder. The flow passing beneath the cylinder enters the combustor, while the flow passing over the cylinder remains outside the engine.

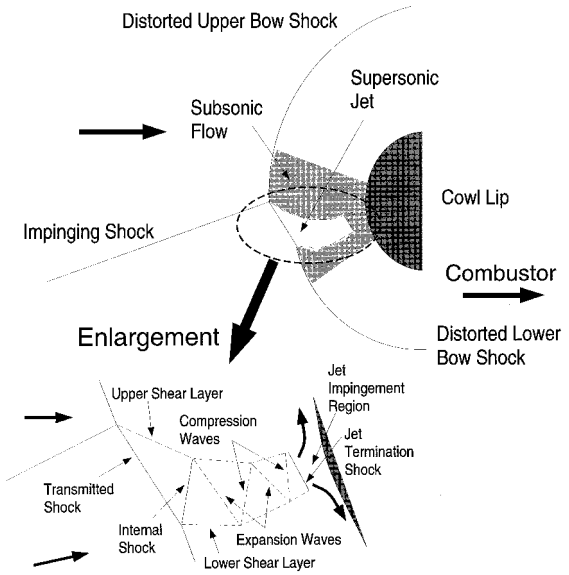

Fig. 1 Schematic of type IV shock interaction, including detail of the supersonic jet.

The type IV interaction is characterized by the bow shock being distorted into two halves, connected by a short, straight, transmitted shock. The flow crossing the upper half of the shock (as shown in Fig. 1) is the freestream, while the flow crossing the lower half of the bow shock and transmitted shock has crossed the impinging oblique shock. Therefore, it is deflected upward, and is at a lower Mach number and higher pressure than the freestream flow. The flow crossing the transmitted shock remains supersonic and is bounded by shear layers, separating it from the subsonic flow that has crossed the bow shock. Emanating from the lower end of the transmitted shock is an oblique shock inside the supersonic jet, which turns that flow parallel to the adjacent subsonic flow. When this oblique shock intersects the upper shear layer, an expansion wave is reflected back, which reflects off the lower shear layer as a compression wave. These weak waves crisscross the jet, alternating between expansions and compressions, until the jet gets close to the body and the supersonic flow is decelerated across a normal shock. Behind the jet termination shock, the subsonic flow is turned along the cylinder surface (Fig. 1).

The early work on the subject of shock interactions were experimental efforts to understand the nose (planar or axisymmetric oblique) shock, and wing or fin leading-edge (transverse bow shock) interaction.[2,3] One objective of this work was to correlate the heating rates as functions of the flow parameters.[2,4] The two-dimensional case with an oblique shock in the same plane as the bow shock is more appropriate for inlet flows with a nose shock-on-cowl lip condition. For this case, it has been demonstrated analytically,[1,5] experimentally,[1–3,5–13] and with computational methods,[14–23] that the point on the cylinder surface where the supersonic jet fluid impinges the body experiences heating rates and peak pressure loads vastly in excess of the stagnation values behind the undistorted bow shock. Furthermore, it has been observed experimentally[7,10,12] and numerically,[15–17,20–22] that under certain circumstances, the jet is unsteady.

While there has been a large amount of experimental and computational fluid dynamics (CFD) simulation of the type IV shock interaction, the cases studied form a limited set of data from the range of possible interactions. Since experimental and numerical analysis are both time-consuming and expensive, it would be extremely difficult to perform wide-ranging parametric studies using these techniques, which would give real insight into what influences the interaction, the physical mechanisms involved, and the range of conditions under which it might take place. Also, it is desirable for engineering purposes to have a quick and economical method for predicting the effects of the interaction. This paper outlines a completely analytical approach to the prediction of the type IV shock interaction, to fulfill these requirements.

Previous Analytical Methods

Initial efforts at simple prediction techniques were essentially correlations for peak pressure and heat transfer. The analysis done by Edney[1] was the first characterization of the six types of interactions, and he produced analytical patterns for each by using the oblique shock relations. The flow in the supersonic jet and the impingement region was modeled by a series of isentropic wave fans, and predictions for the peak pressures and heat transfer because of impingement were given. However, this work was unable to predict the actual size of the jet, and the length of the transmitted shock and jet were taken from experimental results. Edney conducted a series of experiments to support and validate his models.[1]

Keyes and Hains[5] also used the oblique shock relations and Prandtl–Meyer relations to model the six interactions in a similar way, and verified their pressure and heat transfer predictions with experimental results. Their method also required some empirical or experimental values as input. Their systematic modeling of the six types of interaction was compiled into a computer code by Morris and Keyes.[24] The code was extended to include the effects of equilibrium chemistry of air by Glass.[25]

Fully Analytical Solution

Neither of the two methods discussed earlier were truly analytical because an empirical or experimental value was required. The work outlined in this paper extends the methods of Edney[1] and Keyes and Hains,[5] to include the curvature of the bow shock and, hence, determine explicitly the length of the transmitted shock and jet width at termination without any experimental or empirical input.

This model calculates the shock waves and jet structure, and gives a prediction for the peak pressure load and location on a circular cylinder undergoing a type IV shock interaction. The interaction is governed by the freestream (characterized by the Mach number), the impinging shock (characterized by the shock angle or deflection), and a constant that fixes the impinging shock in space.

The model is solved in the following steps (Fig. 2):

1) Given the properties of the freestream flow and the impinging shock angle, the flow properties and directions in regions 1, 2, 3, 4, and 5 can be calculated, as well as the shock wave angles ϕ_A, ϕ_B, ϕ_t, and ϕ_5, by matching pressure and flow directions across the shear layers. After region 5, the properties of the isentropic regions inside the jet (regions 6, 7, etc.) and expansion and compression wave angles ϕ_w are calculated.

2) Initially assuming that there is no distortion caused by the jet, the equation of the lower bow shock can be calculated based on the region 1 flow properties and direction. From the calculated shock-wave angle ϕ_B, the coordinates of the lower end of the transmitted shock (point B) are found.

3) Knowing the spatial equations of the impinging (specified from the initial conditions) and transmitted (known from ϕ_t and the location of B) shocks, the location of the upper end of the transmitted shock (point A), and, hence, its length, can now be calculated, along with all of the expansion and compression waves/shear-layer intersection points (points Q, R, etc.), because the wave slopes are all known and the shear layer slopes match the flow direction.

4) When the jet is aligned normal to the cylinder surface or slightly above the normal, the jet terminates. A normal shock (points Y–Z) decelerates the flow, and the stagnation (impinging) region properties and location can be calculated.

5) The jet fluid is turned away from the stagnation point and traverses along the cylinder surface. If any passes below the

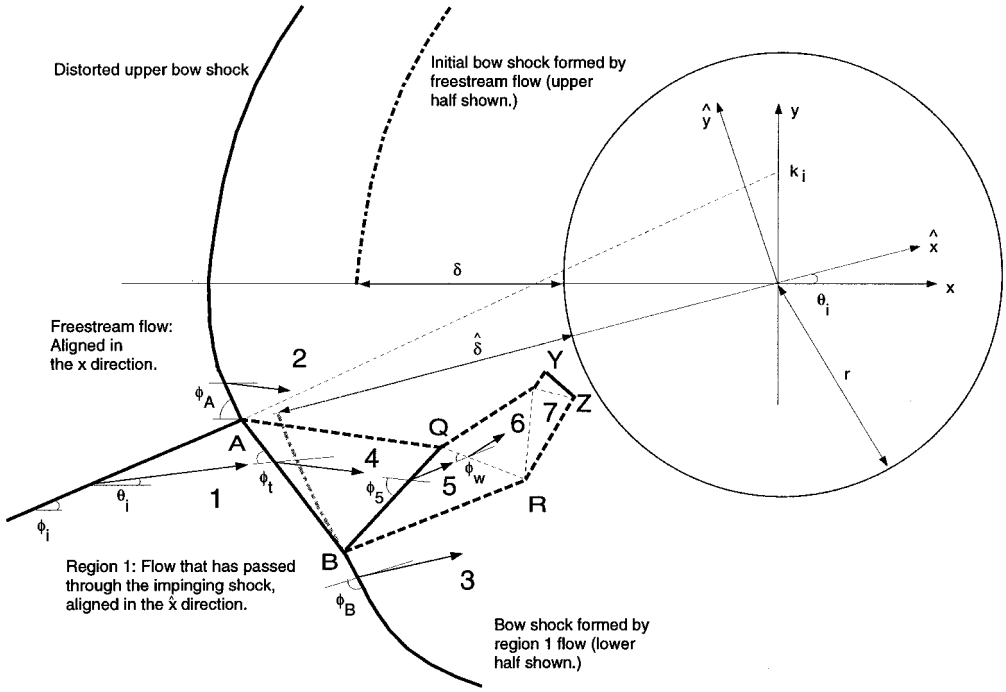

Fig. 2 Schematic showing flow regions, wave angles, and coordinate systems.

cylinder, this stream-tube is used to estimate the lower bow shock distortion (a new value for $\hat{\delta}$). Steps 2–4 can be repeated with a new equation for the lower bow shock until a converged solution for the interaction is obtained.

The analysis performed here is confined to a single shock impinging on the bow shock around a circular cylinder at high Mach numbers. The model assumes a constant ratio of specific heats ($\gamma = 1.4$ for air), and no account is taken of Reynolds number, viscous, or high-temperature effects.

Transmitted Shock and Jet Regions

The first part of the problem involves determining the flow properties and directions and the wave slopes around the jet. The freestream conditions are considered known. Also, the slope and/or flow deflection of the impinging shock are known, and so all conditions in region 1 can be calculated by the standard oblique shock relations[26] (Fig. 2).

In Fig. 2 the upper shear layer emanates from point A, the top of the transmitted shock. Above the shear layer in region 2, the pressure and flow direction must be the same as below the shear layer in region 4. That is, $\theta_2 = \theta_i - \theta_4$ and $P_2 = P_4$. Both of these relations can be written in terms of M_∞, M_1, θ_i, and P_1/P_∞, which are all known; and ϕ_A and ϕ_t, the slopes of the upper bow shock at A and the transmitted shock respectively, which are unknown. They can be solved for ϕ_A and ϕ_t, using an iteration method, since the unknown variables cannot be expressed explicitly.

Now that ϕ_A and ϕ_t are known, the flow properties in regions 2 and 4 can be calculated by the oblique shock relations.

Similarly at point B, in Fig. 2, where the lower shear layer begins: $\theta_5 - \theta_4 = \theta_3$ and $P_3 = P_5$. Again, both of these relations can be written in terms of regions 1 and 4 variables, and ϕ_B and ϕ_5, which are the slopes of the lower bow shock at B and the shock inside the jet, respectively. In exactly the same way as before, we can iteratively solve for ϕ_B and ϕ_5, and, hence, calculate all of the flow properties in regions 3 and 5.

The shock inside the jet emanates from point B and will eventually intersect the upper shear layer at point Q. Because the pressure above the shear layer is assumed to remain constant, the shock will be reflected at Q as an expansion fan. When the expansion waves intersect the lower shear layer (at point R), since the pressure below the shear layer is assumed constant, they will be reflected back as compression waves. These alternating weak expansion and compression waves will keep crossing the jet until the jet ends in a terminating normal shock.

As seen in Fig. 2, because the waves inside the jet, from point Q onward, are weak isentropic expansions and compressions, the total properties will be constant throughout the jet. To maintain constant pressure along the shear layers, the alternate expansions and compressions will turn the flow equal amounts each time, and the Mach number and pressure will alternate between M_5 and P_3 in one region (the odd numbered 5, 7, 9, etc.), and M_6 and P_2 in the adjacent regions (the even numbered 6, 8, etc.). The flow across each expansion or compression wave will be turned up by an angle $\Delta\theta$, where $\Delta\theta = \nu(M_6) - \nu(M_5)$ and $\nu(M)$ is the Prandtl–Meyer function.[26]

The value of M_6 is derived from the isentropic pressure relationship, namely,

$$\frac{P_{06}}{P_6} = \left(1 + \frac{\gamma - 1}{2} M_6^2\right)^{\gamma/(\gamma-1)} \tag{1}$$

where P_6 and P_{06} are known, being equal to P_2 and P_{05}, respectively.

Although the waves are fans of many waves, to simplify the analysis an average slope is assumed, so that intersection points along the shear layers can be calculated. The angles of a compression wave and an expansion wave, relative to the approaching flow, are $\phi_w = (\mu_5 + \mu_6 \pm \Delta\theta)/2$, respectively.

Equation of the Bow Shock

The model (Fig. 3), developed by Moeckel,[27] allows the shape of a detached shock and standoff distance to be predicted, based on the body geometry and freestream Mach number, for axisymmetric and two-dimensional flows. A number of key assumptions are made.

1) The sonic line between the body and shock is assumed to be straight. This is considered valid within the acceptable level of accuracy.

2) The sonic point on the body corresponds to where the local surface inclination is the maximum wedge angle λ_d for

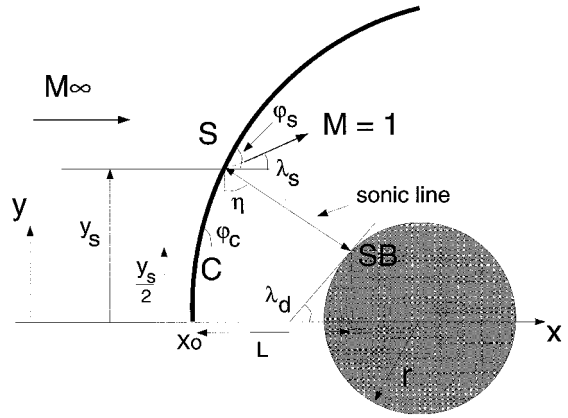

Fig. 3 Model of detached shock.

the freestream Mach number M_∞. Hence, for a cylindrical two-dimensional cowl:

$$y_{SB} = r \cos \lambda_d \tag{2}$$

Although this assertion is not based on rigid, theoretical reasoning, Moeckel[27] does justify it by analogy to sharp cornered bodies.

3) A hyperbolic shape is assumed for the shock, namely,

$$\beta y = \sqrt{x^2 - x_0^2} \tag{3}$$

where $\beta = \sqrt{M_\infty^2 - 1}$, and x_0 is the x coordinate of the shock maximum detachment in the coordinate system used here. The shock slope ς can be expressed as

$$\tan \varsigma = \frac{\sqrt{x_0^2 + \beta^2 y^2}}{\beta^2 y} \tag{4}$$

This form of the shock gives the correct slope at the centerline (the shock should be normal) and at large distances from the body (the shock tends toward a Mach line.)

For a given M_∞, there is a unique shock slope ς_s and flow deflection λ_s, where the Mach number behind the shock is unity, which corresponds to the point S.

The distance L, from x_0 to x_{SB}, can be written as

$$L = x_S + (y_S - y_{SB})\tan \eta - x_0 \tag{5}$$

and substituting for x_S and x_0 from Eqs. (3) and (4) gives

$$L = y_S[\beta(\beta \tan \varsigma_s - \sqrt{\beta^2 \tan^2 \varsigma_s - 1}) + \tan \eta] - y_{SB} \tan \eta \tag{6}$$

To get a value for y_S, continuity can be applied to the stream-tube between the centerline and S, area y_S per unit depth. All of this fluid crosses the sonic line, length $(y_S - y_{SB})/\cos \eta$. An appropriate average value for the properties along the sonic line are those at the mass centroid of the stream-tube, namely, the streamline passing through C, where $y_C = y_S/2$ for two-dimensional flow. Because the total pressure is constant along the streamline behind the shock, and the total temperature is constant everywhere

$$\frac{y_S \cos \eta}{y_S - y_{SB}} = \frac{\Pi_C}{\sigma} \tag{7}$$

where Π_C is the total pressure ratio across the shock at C, and σ is the contraction ratio to decelerate the freestream to sonic velocity isentropically. Hence,

$$y_S = y_{SB}[1 - (\sigma/\Pi_C)\cos \eta]^{-1} \tag{8}$$

The total pressure ratio is expressed in terms of the shock slope and approach Mach number:

$$\Pi_C = \left[1 + \frac{2\gamma}{\gamma + 1}(M_\infty^2 \sin^2 \varsigma_c - 1)\right]^{-1/(\gamma-1)} \times \left[\frac{2 + (\gamma - 1)M_\infty^2 \sin^2 \varsigma_c}{(\gamma + 1)M_\infty^2 \sin^2 \varsigma_c}\right]^{-\gamma/(\gamma-1)} \tag{9}$$

The angle ς_c can be derived from Eq. (4) and $y_C = y_S/2$ as

$$\tan \varsigma_c = \sqrt{4 \tan^2 \varsigma_s - 3/\beta^2} \tag{10}$$

The contraction ratio σ can be expressed as

$$\sigma = \frac{M_\infty}{\sqrt{\left[\left(\frac{2}{\gamma + 1}\right)\left(1 + \frac{\gamma - 1}{2} M_\infty^2\right)\right]^{(\gamma+1)/(\gamma-1)}}} \tag{11}$$

An appropriate value for η is the arithmetic mean of the flow inclinations at S and SB[27]:

$$\eta = (\lambda_s + \lambda_d)/2 \tag{12}$$

Hence, for a given M_∞ and r, it is possible to calculate y_S [Eq. (7)], y_{SB} [Eq. (2)], x_0 [Eq. (4)], and L [Eq. (6)]. The shock detachment δ can be written as

$$\delta = L - r(1 - \sin \lambda_d) \tag{13}$$

Values of δ, and the shock shape obtained with this method, agree closely with those generated by experiment[27] or empirically.[28] Hence, with confidence in the model, it is applied here to the type IV shock-interaction problem.

Bow Shock Distortion

Figure 4 shows a similar model to Fig. 3, with an impinging shock intersecting the bow shock at point A. For the same reasons as discussed earlier, it can be argued that the sonic line is straight from SB to S, and ς_s, λ_s, λ_d, and η are all the same for the given M_∞. Hence, Eqs. (2) and (12) still hold.

The fluid in the stream-tube below A (shaded) will pass through the jet, around the cylinder surface, crossing the sonic line between T and SB, which is a length of A_{s2}. The fluid between y_S and y_A crosses the sonic line between T and S. In the same way as before, we can represent the flow properties along the sonic line between T and S, by an average streamline

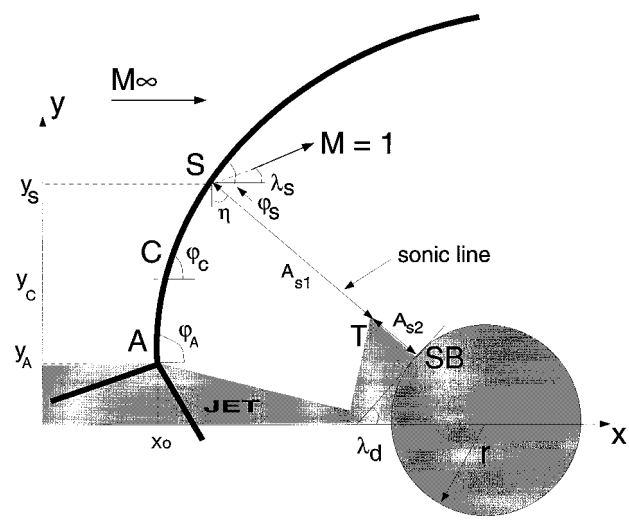

Fig. 4 Detached shock geometry in impinging case.

passing through C, where in two-dimensional flow, $y_c = (y_S - y_A)/2$. Note, that x_0 and ς_c do not have the same values as shown in the preceding text, and Eq. (10) does not hold. However, the equation of the bow shock is still given by Eq. (3). Furthermore, the angle of the bow shock at A is known from the solving the triple point at A.

This leaves six unknowns in the problem: x_0, ς_c, y_S, y_A, y_C, and y_T. If, for now, we know A_{s2}, then

$$y_T = y_{SB} + A_{s2} \cos \eta \tag{14}$$

and $y_C = (y_S - y_A)/2$ can be eliminated from the problem. From Eq. (4)

$$\tan^2 \varsigma_s = \frac{x_0^2 + \beta^2 y_S^2}{\beta^4 y_S^2} \tag{15}$$

$$\tan^2 \varsigma_c = \frac{x_0^2 + \beta^2 (y_S - y_A)^2/4}{\beta^4 (y_S - y_A)^2/4} \tag{16}$$

$$\tan^2 \varsigma_A = \frac{x_0^2 + \beta^2 y_A^2}{\beta^4 y_A^2} \tag{17}$$

and by applying continuity [analogous to Eq. (7)]

$$\frac{(y_S - y_A)\cos \eta}{y_S - y_T} = \frac{\Pi_C}{\sigma} (M_\infty, \varsigma_c) \tag{18}$$

where Π_C and σ are given by Eqs. (9) and (11).

Solving these equations for ς_c gives

$$\tan^2 \varsigma_c = \frac{4\Phi^2(\beta^2 \tan^2 \varsigma_s - 1) + (\Phi - 1)^2}{\beta^2 (\Phi - 1)^2} \tag{19}$$

where

$$\Phi = \sqrt{\frac{\beta^2 \tan^2 \varsigma_A - 1}{\beta^2 \tan^2 \varsigma_s - 1}} \tag{20}$$

and, hence,

$$y_A = \frac{y_T \Pi_C}{\Phi \Pi_C - (\Phi - 1)\sigma \cos \eta} \tag{21}$$

$$y_S = \frac{y_A \sigma \cos \eta - y_T \Pi_C}{\sigma \cos \eta - \Pi_C} \tag{22}$$

The distortion in the bow shock because of the jet fluid can best be measured by the new value for x_0:

$$x_0 = \beta y_S \sqrt{\beta^2 \tan^2 \varsigma_S - 1} \tag{23}$$

Therefore, given A_{s2}, the new x_0 can be calculated.

Transmitted Shock and Jet Geometry

A Cartesian coordinate system is used with the origin at the center of the cylinder. A second coordinate system is aligned parallel to M_1 (Fig. 2). The impinging shock has the equation

$$y = x \tan \phi_i + k_i \tag{24}$$

where k_i is a constant, uniquely defining the location of the shock.

The shock shape model described earlier gives an equation for the curved bow shocks. A modification for the different coordinate systems is needed. For now, we assume the lower bow shock is that generated by a flow at M_1 aligned in the $(\hat{x}, \hat{y})$ directions, namely,

$$\beta_1^2 \hat{y}^2 = \hat{x}^2 + 2(\hat{x}_0 + \hat{\delta} + r)\hat{x} + 2\hat{x}_0(\hat{\delta} + r) + (\hat{\delta} + r)^2 \tag{25}$$

where $\hat{x}_0$ and $\hat{\delta}$ are the Moeckel variables based on M_1 and $\beta_1 = \sqrt{M_1^2 - 1}$. The slope of the bow shock at B, $d\hat{y}/d\hat{x} = \tan \phi_B$, is known, and so the coordinates of B in $(\hat{x}, \hat{y})$ space can be calculated.

The transmitted shock has the equation

$$\hat{y} = k_t - \hat{x} \tan \phi_t \tag{26}$$

where k_t is a constant based on the location of point B in $(\hat{x}, \hat{y})$ space.

The location of point A in $(\hat{x}, \hat{y})$ space can be found by solving Eqs. (24) and (26) (in a consistent coordinate system).

To convert between (x, y) and $(\hat{x}, \hat{y})$:

$$\begin{aligned} \hat{x} &= x \cos \theta_i + y \sin \theta_i \qquad & \hat{y} &= y \cos \theta_i - x \sin \theta_i \\ x &= \hat{x} \cos \theta_i - \hat{y} \sin \theta_i \qquad & y &= \hat{x} \sin \theta_i + \hat{y} \cos \theta_i \end{aligned} \tag{27}$$

Now, we have calculated the locations of points A and B, and the distance between them is the length of the transmitted shock. Since we know all of the angles of waves inside the jet, and the upper and lower shear layers at A and B, respectively, we can solve simple pairs of straight-line equations to calculate the locations of points Q, R, etc. For the purposes of this analysis, the shear layers and waves are considered short, straight, and of negligible thickness.

Jet Termination

Eventually, the jet must terminate with the supersonic flow being decelerated across a normal shock. The flow in the region prior to the termination is known, and the stagnation/impingement region flow properties immediately behind the normal shock can be calculated by the normal shock relations.[26] The termination is assumed to occur when either an intersection point between an internal Prandtl–Meyer wave and the shear layers would be inside the cylinder surface, or when the jet flow is almost normal to the surface. When this is the case, the pressure behind the normal shock is the highest as the impinging flow on the cylinder surface will be a stagnation region as opposed to a grazing stream-tube. When the jet flow is aligned away from the surface, by a significant angle, there is pressure relieving as the flow turns over the cylinder, which may prevent a normal shock forming.

In each region of the jet, a terminating shock could be drawn, normal to the flow direction in that region. The velocity vectors of the flow crossing the shock will intersect the cylinder surface at a range of surface angles. Consider Fig. 5a, which shows a terminating shock ($Y - Z$), where one of the flow vectors strikes normal the surface. In this case, the model of the jet would end with a normal shock and impingement at a stagnation point. The flow would be split with some fluid passing over the top of the cylinder and some passing over the bottom. The amount of flow either way can be measured in terms of the areas of the terminating shock either side of the normal line, A_{T1} and A_{T2}. The impingement point would be where the flow is normal to the surface, and the peak pressure would be the stagnation pressure. The impingement point is usually given as an angle measured from the front face of the cylinder [point $(-r,0)$].

If all of the flow vectors between Y and Z in a given jet region intersected the surface below the surface normal, which is parallel to the jet flow, the model would proceed to generate the next region of the jet. If all of the flow vectors intersect the surface above the surface normal that is parallel to the jet flow, it is a sign that the jet has turned the flow past a stag-

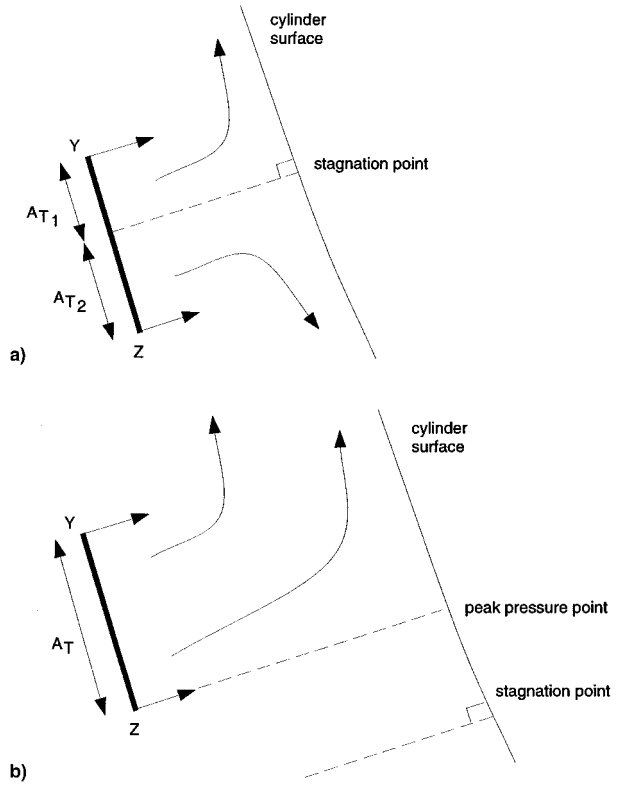

Fig. 5 Jet terminating shock: a) impinging flow is normal to surface and b) impinging flow grazes top of the cylinder.

nation-type impingement, as described earlier. Additional regions will only turn the flow further away, and so the jet is terminated at this point. There is a slight distance between the normal to the surface, which is parallel to the flow and the intersection of the flow vector through point Z (Fig. 5b). One possibility (which is applied here), is to neglect this distance and let the peak pressure equal the stagnation pressure, acting on the cylinder below Z. However, in actuality, the flow passing through the normal shock is turned, passing over the cylinder, so that there is some relieving of the pressure.

Although this situation bears some resemblance to an incompressible flat-plate stagnation flow, such a model relies on boundary conditions at infinity that are not applicable in this case. Using the conditions behind the normal shock as boundary conditions results in an estimate for the peak pressure, which potentially could be too low or even negative.

Iteration Step

If the flow impinging on the cylinder split with some fluid passing over the bottom half, as shown in Fig. 5a, the lower bow shock would, in fact, be distorted, and the initial assumption of Eq. (25) would need to be modified as described earlier.

The locations of points Y and Z are known, and so the distance between them is the length of the terminating shock A_T. The value of A_{T2} can also be calculated from geometrical relations. The Mach number behind the termination shock is known, M_{stag}. If all of the fluid crossing A_{T2} moves isentropically over the cylinder to the sonic line SB–T (Fig. 4), then from the area-Mach number relationship:

$$\frac{A_{T2}}{A_{s2}} = \frac{1}{M_{\text{stag}}} \sqrt{\left[\left(\frac{2}{\gamma+1}\right)\left(1+\frac{\gamma-1}{2}M_{\text{stag}}^2\right)\right]^{(\gamma+1)/(\gamma-1)}} \tag{28}$$

Hence, we can calculate A_{s2}. The new values of $\hat{x}_0$ and $\hat{\delta}$ can be found using Eqs. (14)–(23), except with point A in Fig. 4, being point B on the transmitted shock in $(\hat{x}, \hat{y})$ space. Recalculating the length of the transmitted shock and internal structure of the jet will modify the impingement region, which might make several iterations necessary for calculating the distortion in the lower bow shock before an unchanging solution is obtained.

Validation

To validate this analytical model, a number of test cases were run for which there were published data for the interactions. Four experimental shock interactions, which were performed by Holden et al.[10] in the Calspan 48- and 96-in. shock tunnels at approximately Mach 8, were chosen. A 1.5 in. (3.81 cm) radius cylinder was used for generating the detached shock, and a 12.5-deg wedge was used for generating the oblique shock. The wedge position was changeable, giving different values of k_i. The test conditions are summarized in Table 1. The pressure coefficient is defined as the ratio of measured peak pressure on the cylinder surface to the freestream dynamic pressure.

In all four analytical computations, the jet terminated just above the surface normal line, meaning no iteration for the distortion in the lower bow shock was necessary. However, this also means the calculated peak pressures should include some relieving, and, hence, they would tend to overpredict the peak pressure slightly. There is good agreement between the experimental and analytical results for pressure coefficient and impingement angle. Figure 6 shows the comparison between the analytical shock shapes and jet and the schlieren picture from the experimental report for run 24. The overall shock pattern shows good agreement. Similar agreement is obtained in the other three cases. It is worth noting the variation in impingement shock angle, which results from the viscous interaction on the shock-generating wedge. The nature of schlieren photographs and the quality of reproduction make it difficult to determine exactly the edge of the cylinder and the shock waves; hence, the imprecise estimates for L_t in Table 1. Although there are no quoted transmission shock lengths, the agreement appears to be good. Overall, it can be seen that the analytical predictions are very close to the experimental results. The entire calculation was completed in a fraction of a second on a desktop workstation.

Parametric Study

A series of solutions were generated for different values of k_i, θ_i, and M_∞. A cylinder with a radius of 3.81 cm was used for each case. The values of k_i were varied from 1.2 to 2.2 cm, θ_i was set at either 10, 12.5, or 15 deg, and M_∞ was set at either 6, 8, or 10.

The values of peak impingement pressure ratio on the cylinder are summarized in Table 2. The pressure ratio is the peak-impinging pressure on the cylinder divided by the stagnation pressure behind the bow shock at the centerline, if there were no impingement. There is no difference in the pressure values as k_i varies, because in each case, the jet is terminating in the same type (odd or even) of region and no account is taken of any possible pressure relieving. In the case of M_∞ = 6 and θ_i = 10 deg, a different value was obtained for k_i greater than 1.8 cm (6.931), as opposed to below 1.8 cm (5.252), because the jet is terminating in a different type of region in each case. It can be seen that as the freestream Mach number increases, so does the peak pressure. There is little change in pressure for different values of θ_i.

Figures 7–9 show the variations in jet impingement angle, transmitted shock length, and jet terminating shock length. Several observations can be made. As the value of k_i increases, the values of all three variables increases with a few exceptions. In two cases, M_∞ = 6, θ_i = 12.5 deg and M_∞ = 8, θ_i = 10 deg, there is no variation in jet impingement angle with k_i. This occurs because in the analytical model, the jet is terminating exactly normal to the surface. Although the fluid passing below the cylinder is distorting the shock (which is accounted for), and with different k_i, a different amount of

Table 1 Experimental cases used for model validation

			Experiment			Analytic		
Run[a]	M_∞	k_i, cm	C_p	θ_{inp}, deg	Lt/r[b]	C_p	θ_{inp}, deg	Lt/r
21	8.03	1.32	14.2	17.7	0.4	14.8	16.7	0.421
22	7.95	1.39	12.5	15.8	0.5	14.6	17.1	0.448
24	8.14	1.22	12.1	18.3	0.5	15.0	16.1	0.385
60	8.04	1.56	15.7	19.1	0.6	14.8	17.6	0.514

[a]Run numbers refer to experiments performed by Holden et al.[10] [b]Measured from schlieren photographs.

Table 2 Peak pressure ratios for different interaction cases

	θ_i, deg		
M_∞	10	12.5	15
6	6.931/5.252	5.712	5.859
8	7.471	7.955	7.945
10	9.436	9.790	9.531

Fig. 6 Comparison with experimental result: run 24 (Ref. 10).

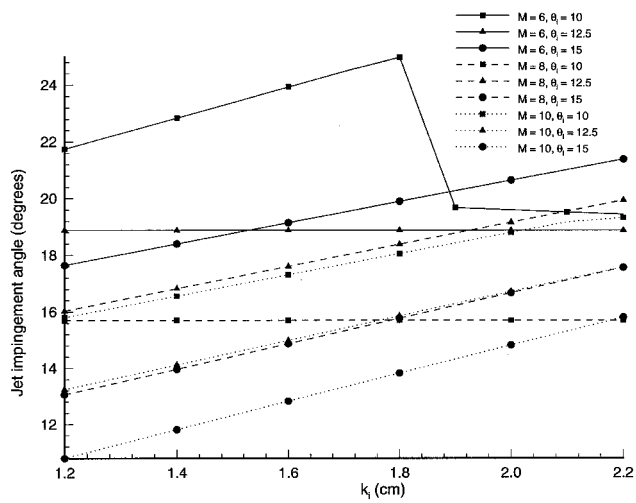

Fig. 7 Jet impingement angle for different cases.

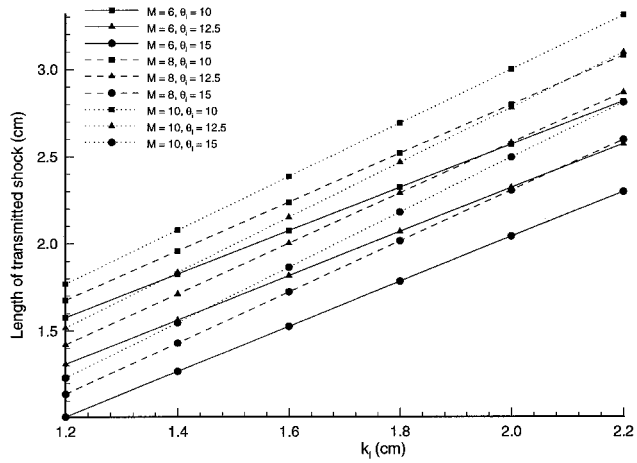

Fig. 8 Length of transmitted shock for different cases.

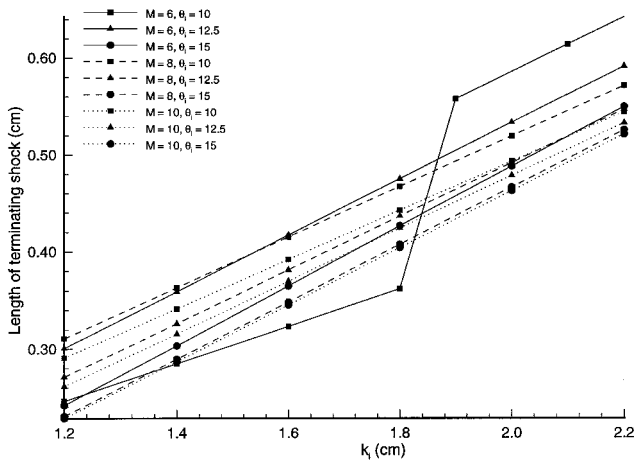

Fig. 9 Length of terminating shock for different cases.

fluid passes each way; in every case, the peak pressure point is taken to be the stagnation point where the flow is normal to the surface.

Although the three variables shown in Figs. 7–9 show a generally linear trend, a noticable discontinuity occurs in the case of $M_\infty = 6$ and $\theta_i = 10$ deg, for the same reasons as mentioned earlier. The reason for this is that below $k_i = 1.8$ cm, the jet is terminating in region 7, with all of the fluid passing over the upper half of the cylinder. When k_i is greater than 1.8 cm, the jet terminates in region 6, with the fluid passing below the cylinder. An interesting phenomenom occurs when $k_i = 1.8$ cm. The analytical model cannot converge on a single solution when the distortion in the lower bow shock is accounted for. Instead, the iteration moves between two different solutions, summarized in Table 3. The region 7 termination case is plotted in Figs. 7–9. This case has the jet striking normal to the surface. The part of the jet fluid that distorts the lower bow shock results in a new jet position that is forced to terminate in region 6, with the jet fluid entirely passing beneath the cylinder. This new distortion in the bow shock results in a new jet position, which is the same as the original region 7 terminating case. Whether this phenomenom (unique to this one case) is a quirk of the analytical equations used in this method, or a genuine representation of some physical unsteadiness, is unclear. In each case, the analytical method is matching physical properties such as pressure and continuity.

With everything else being constant, the effect of increasing Mach number or θ_i, with the same exceptions as shown earlier, seems to increase the length of the transmitted shock and de-

Table 3 Two solutions for the case with $M_\infty = 6$, $u_i = 10$ deg, and $k_i = 1.8$ cm

	Case 1	Case 2
Termination region	7	6
L_s, cm	2.324	2.315
A_T, cm	0.362	0.528
θ_{inp}, deg	25.0	18.5
Pressure ratio	6.93	5.25

Table 4 Results with different cylinder radii

r, cm	%[a]	L_s, cm	%[a]	θ_{inp}, deg	%[a]	A_T, cm	%[a]
3.048	−20	1.771	3.7	18.4	8.0	0.337	3.4
3.810	0	1.707	0	17.0	0	0.326	0
4.572	20	1.646	−3.6	16.1	−5.4	0.314	−3.7
5.334	40	1.584	−7.2	15.4	−9.2	0.302	−7.4

[a]Percentage change from baseline case.

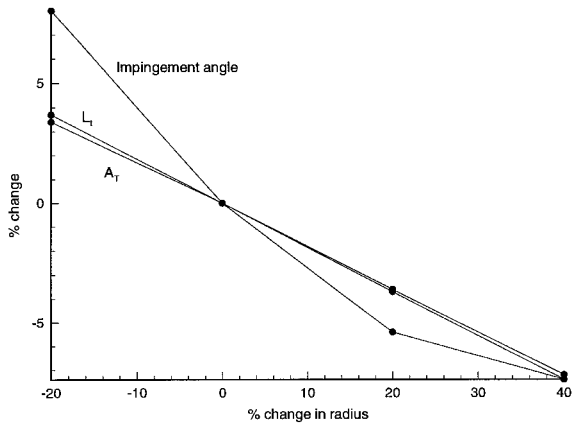

Fig. 10 Variation in impingement angle, transmitted shock, and terminating shock lengths with changing radius.

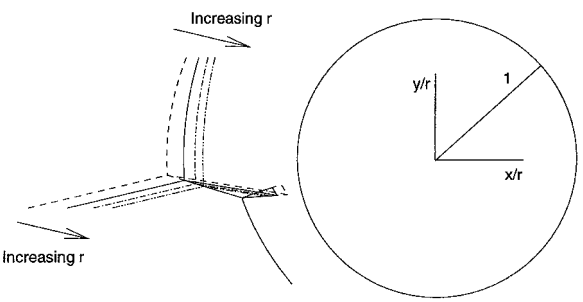

Fig. 11 Interaction patterns for varying radii cases scaled by radius.

crease the width of the terminating shock and impingement angle.

Another series of solutions was generated for cylinders of different radii. A baseline configuration was chosen with the 3.81 cm radius cylinder at Mach 8. A fixed impinging shock was generated with $\theta_i = 12.5$ deg and $k_i = 1.39$ cm. The cylinder radius was then reduced by 20%, and increased by 20 and 40% while keeping the freestream conditions and impinging shock the same. The results are summarized in Table 4. The peak pressure ratio in each case was 7.95, which did not change with radius for the same reasons as previously outlined.

As the radius is increased, the bow shocks are displaced proportionally further outward. This is to be expected, since the bow shock detachment distance is proportional to the cylinder radius. Figure 10 shows the variation in impingement angle, transmitted shock, and terminating shock lengths with changing radius. The effect of increasing the cylinder radius, for given freestream conditions and a given impinging shock, is to reduce the jet width (as measured by the transmitted shock length or terminating shock length) linearly. A 10% increase or decrease in radius leads to about a 1.8% decrease or increase, respectively, in jet width. The relationship between change in jet width and radius is not one-to-one, which can be explained by considering Fig. 11. Figure 11 shows the four patterns scaled spatially by the cylinder radius for that case, along with a nondimensionalized cylinder of radius 1. Because the lower bow shock is unaffected by the interaction, since the jet fluid passes over the top of cylinder, all four curves scale directly with radius and coincide. However, the four impinging shocks, which would be identical in an unscaled comparison since they are fixed in space, are scaled differently. Hence, the effect of increasing the cylinder radius is analogous to moving the impinging downward, and the overall pattern does not scale completely with radius. Increasing the radius also seems to result in a lower (i.e., closer to the centerline) impingement angle. The reverse is true for a decreased radius. These trends are consistent with those seen in the earlier parametric study.

This type of parametric study highlights the usefulness of this analytical model. The radius of the cowl lip is a key variable for the design of the inlet. Similarly, the width of the jet at termination, and the peak pressure load and location, are key design inputs for structural and thermal design.

Conclusions

A model has been developed and validated that predicts the type IV shock interaction at hypersonic Mach numbers in calorically perfect air. By calculating the shape of the curved bow shocks, no empirical or experimental information about the jet is required. The length of the transmitted shock and width of the jet are calculated directly. This is the first completely analytical method not requiring empirical or experimental data to be developed for the type IV shock interaction. It allows a comprehensive parametric study of the interaction to be conducted. The model, which is extremely quick to complete a full calculation, can be used as a practical and economical engineering design tool, and also used to obtain physical insight into the interaction.

One such example of this was a parametric study demonstrating the variation of key interaction results, such as peak pressure, impingement location, and the lengths of the transmitted and terminating shocks because of impinging shock location, strength, freestream Mach number, or cylinder radius. Many discernible trends are apparent, such as mostly linear relationships in the dependent variables as the impinging shock is moved, or equivalently when the cylinder radius is changed.

The next step for this research is to extend the method to include noncircular cross section (power law) bodies. These solutions will need CFD validation since no research to date has examined the type IV shock interaction on these types of shapes. Other extensions to the method will include a more satisfactory modeling of the jet impingement region, including some measure of the effect of pressure relieving, and an estimate of the heat loading at the impingement point. In addition, the method could include analysis of the effects of high temperature and chemically reacting air, and modeling of the shear layers and their structure and stability, to answer the question of why the jet appears unsteady under certain circumstances.

Acknowledgments

This research was supported by the Center for Hypersonics Education and Research at the University of Maryland (NASA NAGw 11796). The Technical Monitor was Isaiah Blankson, and appreciation is expressed for this support. The authors would like to acknowledge Robert Nowak, of the NASA Langley Research Center, for the initial idea for this work.

References

[1]Edney, B., "Anomalous Heat Transfer and Pressure Distributions on Blunt Bodies at Hypersonic Speeds in the Presence of an Impinging Shock," Aeronautical Research Inst. of Sweden, FFA Rept. 115, Stockholm, Sweden, Feb. 1968.

[2]Francis, W. L., "Experimental Heat-Transfer Study of Shock Impingement on Fins in Hypersonic Flow," *Journal of Spacecraft and Rockets*, Vol. 2, No. 4, 1965, pp. 630–632.

[3]Hiers, R. S., and Loubsky, W. J., "Effects of Shock-Wave Impingement on the Heat Transfer on a Cylindrical Leading Edge," NASA TM D-3858, Feb. 1967.

[4]Keyes, J. W., and Morris, D. J., "Correlations of Peak Heating in Shock Interference Regions at Hypersonic Speeds," *Journal of Spacecraft and Rockets*, Vol. 9, No. 4, 1972, pp. 621–623.

[5]Keyes, J. W., and Hains, F. D., "Analytical and Experimental Studies of Shock Interference Heating in Hypersonic Flow," NASA TN D-7139, May 1973.

[6]Wieting, A. R., "Experimental Study of Shock Wave Interference Heating on a Cylindrical Leading Edge," NASA TM-100484, May 1987.

[7]Holden, M. S., Wieting, A. R., Moselle, J. R., and Glass, C., "Studies of Aerothermal Loads Generated in Regions of Shock/Shock Interaction in Hypersonic Flow," AIAA Paper 88-0477, Jan. 1988.

[8]Glass, C. E., Holden, M. S., and Wieting, A. R., "Effect of Leading Edge Sweep on Shock-Shock Interference at Mach 8," AIAA Paper 89-0271, Jan. 1989.

[9]Wieting, A. R., and Holden, M. S., "Experimental Study of Shock Wave Interference Heating on a Cylindrical Leading Edge at Mach 6 and 8," *AIAA Journal*, Vol. 27, No. 11, 1989, pp. 1557–1565.

[10]Holden, M. S., Moselle, J. R., and Lee, J., "Studies of Aerothermal Loads Generated in Regions of Shock/Shock Interaction in Hypersonic Flow," NASA CR-181893, Oct. 1991.

[11]Holden, M. S., and Nowak, R. J., "Studies of Shock/Shock Interaction on Smooth and Transpiration-Cooled Hemispherical Nosetips in Hypersonic Flow," AIAA Paper 91-1765, June 1991.

[12]Holden, M. S., and Kolly, J. M., "Measurements of Heating in Regions of Shock/Shock Interaction in Hypersonic Flow," AIAA Paper 95-0640, Jan. 1995.

[13]Kolly, J. M., "An Investigation of Aerothermal Loads Generated in Regions of Hypersonic Shock Interference Flows," Ph.D. Dissertation, Univ. at Buffalo, State Univ. of New York, Buffalo, NY, 1996.

[14]Tannehill, J. C., Holst, T. L., Rakich, J. V., and Keyes, J. W., "Comparison of a Two-Dimensional Shock Impingement Computation with Experiment," *AIAA Journal*, Vol. 14, No. 4, 1976, pp. 539–541.

[15]Klopfer, G. H., and Yee, H. C., "Viscous Hypersonic Shock-on-Shock Interaction on Blunt Cowl Lips," AIAA Paper 88-0233, Jan. 1988.

[16]Singh, D. J., Kumar, A., and Tiwari, S. N., "Influence of Shock Interactions on the Blunt Body Flow Field at Hypersonic Flight Speeds," AIAA Paper 89-2184, July 1989.

[17]Gaitonde, D., and Shang, J. S., "A Numerical Study of Viscous Shock-on-Shock Hypersonic Flows with a Modified Steger-Warming Flux Split Scheme," AIAA Paper 90-1491, Jan. 1990.

[18]Prabhu, R. K., "An Implementation of a Chemical and Thermal Nonequilibrium Flow Solver on Unstructured Meshes and Application to Blunt Bodies," NASA CR-194967, Aug. 1994.

[19]Vemaganti, G. R., "Laminar and Turbulent Flow Computations of Type IV Shock-Shock Interference Aerothermal Loads Using Unstructured Grids," NASA CR-195008, Oct. 1994.

[20]Zhong, X., "Application of Essentially Nonoscillatory Schemes to Unsteady Hypersonic Shock-Shock Interference Heating Problems," *AIAA Journal*, Vol. 32, No. 8, 1994, pp. 1606–1616.

[21]Lind, C. A., and Lewis, M. J., "Unsteady Characteristics of a Hypersonic Type IV Shock Interaction," *Journal of Aircraft*, Vol. 32, No. 6, 1995, pp. 1286–1293.

[22]Lind, C. A., and Lewis, M. J., "Computational Analysis of the Unsteady Type IV Shock Interaction of Blunt Body Flows," *Journal of Propulsion and Power*, Vol. 12, No. 1, 1996, pp. 127–133.

[23]Carlson, A. B., and Wilmoth, R. G., "Monte Carlo Simulation of a Near-Continuum Shock-Shock Interaction Problem," *Journal of Spacecraft and Rockets*, Vol. 31, No. 1, 1994, pp. 25–30.

[24]Morris, D. J., and Keyes, J. W., "Computer Programs for Predicting Supersonic and Hypersonic Interference Flow Fields and Heating," NASA TM X-2725, May 1973.

[25]Glass, C. E., "Computer Program Which Solves Two-Dimensional Shock Wave Interference Problems Using an Equilibrium Chemically Reacting Air Model," NASA TM-4187, Aug. 1990.

[26]Liepman, H. W., and Roshko, A., *Elements of Gasdynamics*, Wiley, New York, 1957.

[27]Moeckel, W. E., "Approximate Method for Predicting Form and Location of Detached Shock Waves Ahead of Plane or Axially Symmetric Bodies," NACA TN D-1921, July 1949.

[28]Billig, F. S., "Shock-Wave Shapes Around Spherical- and Cylindrical-Nosed Bodies," *Journal of Spacecraft and Rockets*, Vol. 4, No. 6, 1967, pp. 882, 823.